aerospace

MDPI

Article

Exploration of Solar Power System Integration for Sustainable Air Transportation—A Case Study for Seaplane Air Taxi Operations

Susan Liscouët-Hanke [1,*], Mohammad Mir [2] and Musavir Bashir [2]

[1] Department of Mechanical, Industrial and Aerospace Engineering, Concordia Institute of Aerospace Design and Innovation, Concordia University, Montreal, QC H3G 1M8, Canada
[2] Department of Mechanical, Industrial and Aerospace Engineering, Concordia University, Montreal, QC H3G 1M8, Canada
* Correspondence: susan.liscouet-hanke@concordia.ca

Abstract: To reduce the environmental impact of airborne transportation, the aeronautic community investigates smaller aircraft with short-range operations (such as training aircraft, air taxis, or commuter aircraft) as technology incubators. This paper contributes to this effort by presenting an analysis framework and a detailed case study for integrating an auxiliary solar power system for air taxi operations. The solar power system conceptual design and analysis framework is improved to capture important effects for more realistic analysis for smaller aircraft, such as allowing the solar power system's efficiency to be estimated as a function of aircraft mission parameters (temperature, speed, cloudiness) and providing a detailed view of the new system's weight estimation considering potential physical integration scenarios. A detailed analysis of Harbour Air's seaplane air taxi operations and the DHC-2 Beaver is performed using this enhanced design framework. The results show that the solar power system output exceeds the required secondary electrical power for 86% of the mission in one season; hence, it provides the potential to supplement a hybrid electric propulsion system. Secondly, the authors designed experiments to investigate the sensitivity of technology uncertainties for one critical mission. The results show that a small fuel burn reduction can be achieved with current technologies, with a promising trend of more savings with increasing system efficiency. Also, the results show that accumulated over a season's operation, the CO_2 emissions from the aircraft can be reduced. The findings indicate that integrating solar power systems can supplement traditional power sources and improve ground operations: specifically, solar energy could power a zero-emission and autonomous air-conditioning system while parked. Overall, integrating solar power into seaplane air taxi operations, even as a retrofit, presents a viable strategy for achieving more sustainable air transportation.

Keywords: aircraft design; auxiliary solar power system; seaplane air taxi; photovoltaic system

check for updates

Academic Editor: Giuseppe Palaia

Received: 20 December 2024
Revised: 13 February 2025
Accepted: 14 February 2025
Published: 20 February 2025

Citation: Liscouët-Hanke, S.; Mir, M.; Bashir, M. Exploration of Solar Power System Integration for Sustainable Air Transportation—A Case Study for Seaplane Air Taxi Operations. *Aerospace* **2025**, *12*, 164. https://doi.org/10.3390/aerospace12030164

Copyright: © 2025 by the authors. Licensee MDPI, Basel, Switzerland. This article is an open access article distributed under the terms and conditions of the Creative Commons Attribution (CC BY) license (https://creativecommons.org/licenses/by/4.0/).

1. Introduction

To reduce the environmental impact of airborne transportation, the aeronautic community investigates smaller aircraft with short-range operations (such as training aircraft, air taxis, or commuter aircraft) as technology incubators, primarily focusing on electric propulsion [1] and hydrogen-based propulsion [2].

Solar power as an alternative propulsion system has been investigated mainly in experimental aircraft [3,4], unmanned air vehicles [5,6], and recently for airships [7,8]. Examples such as the Zephyr [9], which can stay aloft for weeks, or the round-the-world flight of the Solar Impulse 2 [10] indicate a promising path for the industry.

Despite recent advancements in solar cell efficiency, with the National Renewable Energy Laboratory reporting over 26% for silicon cells and 47% for multi-junction cells, highlighting the potential for solar energy in aviation [11], scaling the solar power concept to larger aircraft remains a challenge due to exponential increase in propulsive power [12] and challenges associated with current photovoltaic technologies, such as weight associated with limited power output. In addition, structural integration must not compromise aerodynamic efficiency or structural integrity, temperature management and advanced cooling systems are needed to dissipate heat generated by solar panels, and for long-endurance operation, energy storage solutions must address limitations in battery energy density and weight [13]. Furthermore, the availability of solar radiation is inconsistent, fluctuating based on the time of day, geographic location, season, and weather conditions.

Therefore, the concept of a supplemental or auxiliary solar power system (SPS) [14] is promising as a technology insertion strategy, as investigated in several studies [12,13,15], showing potential for smaller aircraft with daylight operations. In addition, some studies have investigated hybrid propulsion systems, combining batteries and solar cells or batteries, solar cells, and fuel cells to enhance feasibility [16,17]. These hybrid approaches are promising in addressing energy storage limitations and ensuring continuous power supply during varying flight conditions.

Numerous studies have focused on enhancing the efficiency and reliability of SPS through improved solar cell technologies, innovative cooling strategies, and robust energy management systems [18,19]. Several research papers have addressed the development of design, analysis, and power output prediction models [15,20,21] to support feasibility studies, and several have addressed the improvement of certain aspects, such as partial shading [22] or thermal impact on solar cell efficiency [23].

Summarizing the insights from prior studies, seasonal daylight operation of air taxis, particularly seaplanes, mainly using high-wing aircraft configurations, seems conducive to SPS integration, minimizing shading effects to maximize solar energy absorption capabilities. Seaplanes are aircraft designed to take off and land on water, utilizing their hulls or floats for buoyancy. Research on seaplanes highlights their dual land and water utility, which is valuable in areas with abundant water surfaces. Seaplane transport potential for the future is supported by a study focusing on Greece [24], attesting to enhanced sustainable transport and connectivity. In North America, particularly Canada, the prevalence of water bodies supports active seaplane traffic, exemplified by the Vancouver Harbour seaplane seaport [25]. Air taxis, small aircraft used for short-distance travel within urban environments, are also gaining attention as a solution to urban congestion. Advancing aerodynamics, materials, and propulsion systems have renewed interest in seaplanes, making them suitable for environmental monitoring, medical evacuation, and freight transport to remote communities [26–28].

Given the growing need to reduce the environmental impact of aviation, investigating the integration of solar power systems in seaplanes, sightseeing air taxis, and recreational aircraft like the DHC-2 Beaver and Twin Otter is relevant. These aircraft face increasing pressure to minimize their carbon footprint, as seen with Harbour Air's e-Beaver initiative, which aims to electrify its fleet [29]. Therefore, this paper aims to gain new insights on the viability of SPSs for these aircraft types and the potential to reduce their environmental impact from operations. In particular, this paper aims to answer whether retrofitting seaplane air taxis with an SPS would reduce their environmental impact and what benefits can be reached in an electrified aircraft variant.

First, an enhanced SPS design and analysis tool and a multidisciplinary analysis and optimization (MDAO) framework are presented in Section 2, adapted for seaplane aircraft analysis. In Section 3, we conduct an in-depth study of Harbour Air's operations to achieve this

goal, as mission data are readily available to the public, followed by a design-of-experiment analysis for varying technology parameters, followed by a conclusion in Section 4.

2. Methodology

To analyze the viability and potential of a solar power system for air taxi–seaplane operation, the authors use an improved version of a solar system sizing tool based on prior work by the research group [14,15] and an MDAO framework for aircraft-level analysis. The conceptual design framework depicted in Figure 1 focuses on analyzing the impact of an SPS on the aircraft. It is suited to integrating into typical MDAO frameworks for aircraft conceptual design. Details about this design framework and the underlying equations are provided in [15]. The following subsections briefly describe this design framework, highlighting novel aspects integrated for smaller aircraft.

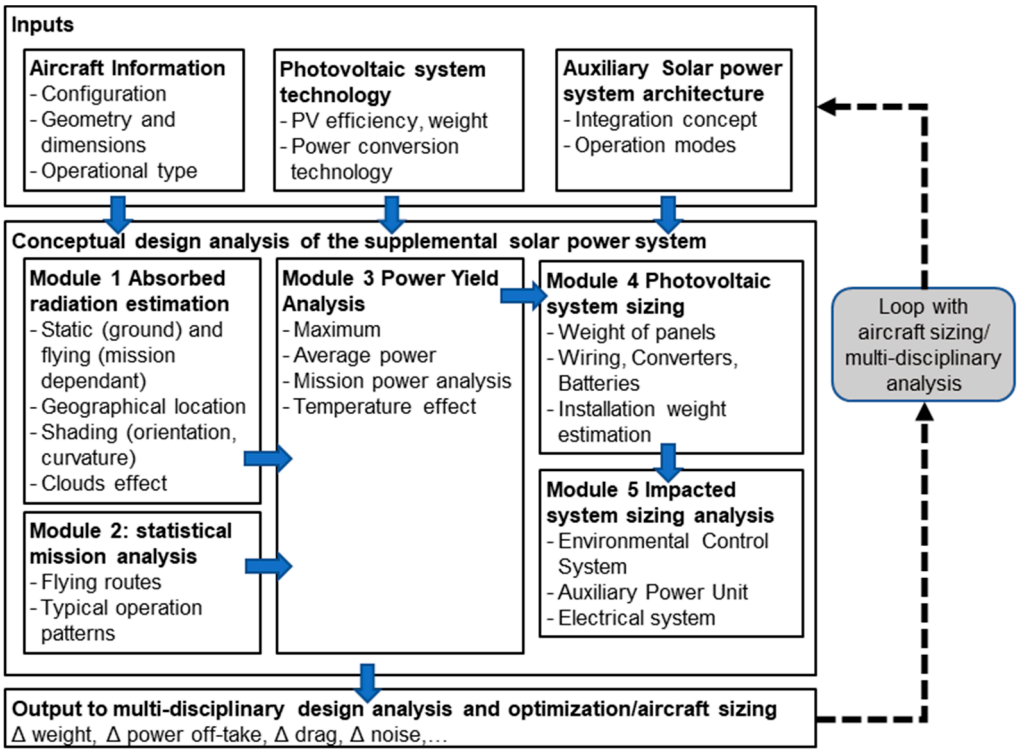

Figure 1. Sizing and analysis framework for solar power systems, adapted from [12,15].

This section first describes the improvements in the solar system sizing tool (Section 2.1) followed by the details of the MDAO integration (Section 2.2).

2.1. Solar System Sizing and Analysis Framework

Module 1 contains the models and methods to calculate the absorbed radiation in various operation scenarios. Module 2 focuses on understanding how the flight mission pattern impacts the power yield of the SPS. Variations in routes, operation time, and schedule can significantly affect overall power yield, potentially rendering the solution non-viable. Module 3 combines inputs from Modules 1 and 2 for power yield analysis, including solar cell technology and additional SPS equipment. Module 4 examines the architecture of aircraft systems after adding solar power systems. Module 5 estimates SPS weight, considering aircraft geometry and wiring. Module 6 is reserved for analyzing impacts on other aircraft systems based on SPS implementation.

To perform the case study for the seaplane operation, the authors expanded Modules 1, 3, and 4 of the framework.

2.1.1. Module 1 Improvements: Solar Irradiance Model

One must consider four factors to calculate absorbed radiation by solar cells on an aircraft: geographical location, cell orientation to the sun, potential shading, and meteorological conditions. The mathematical model calculates the absorbed radiation during a flight mission between two locations for the aircraft's tail, wing, and/or fuselage, as the continuation of previous work from our lab.

The solar declination angle δ [30,31], which varies with the day of the year n, is given by Equation (1):

$$\delta = 23.45^\circ \cdot sin\left(\frac{360^\circ \cdot (284 + n)}{365} \cdot \frac{\pi}{180^\circ}\right) \quad (1)$$

The absorbed radiation during a flight mission is calculated between two locations, and the changes in latitude ϕ and longitude λ between the departure and arrival points are given by Equations (2) and (3).

$$\Delta\phi = \phi_{arr} - \phi_{dep} \quad (2)$$

$$\Delta\lambda = \lambda_{arr} - \lambda_{dep} \quad (3)$$

Moreover, the sun radiation power density [W/m^2] received by the aircraft depends on the angle between the vector pointing to the sun and its projection on a horizontal plane. This azimuth angle (β) is given by Equation (4).

$$\beta = tan^{-1}\left(\frac{X}{Y}\right) \quad (4)$$

$$X = cos(\phi_{arr}) \cdot sin(\lambda_{arr} - \lambda_{dep}) \quad (5)$$

$$Y = cos(\phi_{dep}) \cdot sin(\phi_{arr}) - sin(\phi_{dep}) \cdot cos(\phi_{arr}) \cdot cos(\lambda_{arr} - \lambda_{dep}) \quad (6)$$

Since the irradiance changes with the location, the latitude and longitude are calculated at each time step i during the flight using Equations (7)–(9).

$$\phi[i] = \phi_{dep} + \left(\frac{\Delta\phi}{T_{hour}}\right) \cdot \left(\frac{10i}{60}\right) \quad (7)$$

$$\lambda[i] = \lambda_{dep} + \left(\frac{\Delta\lambda}{T_{hour}}\right) \cdot \left(\frac{10i}{60}\right) \quad (8)$$

$$cos(\theta)[i] = sin\left(\frac{\phi[i] \cdot \pi}{180}\right) \cdot sin\left(\frac{\delta \cdot \pi}{180}\right) + cos\left(\frac{\phi[i] \cdot \pi}{180}\right) \cdot cos\left(\frac{\delta \cdot \pi}{180}\right) \cdot cos\left(\frac{HRA[i] \cdot \pi}{180}\right) \quad (9)$$

The cosine of the solar zenith angle, the solar zenith angle, and the air mass [32] are crucial for calculating the intensities of solar radiation at each time step. These parameters directly influence the beam, direct, diffuse, and incident intensity of solar radiation. These are given by Equations (10) and (11).

$$\theta[i] = cos^{-1}(sin(\theta)[i]) \cdot \frac{180}{\pi} \quad (10)$$

$$AM[i] = \frac{1}{cos(\theta)[i] + 0.50572 \cdot (96.07995 - \theta[i])^{-1.6364}} \quad (11)$$

Finally, the beam intensity I_{beam} [33], direct intensity I_{direct}, diffuse intensity $I_{diffuse}$, and incident intensity $I_{incident}$ of solar radiation for each time step are computed using Equations (12)–(15).

$$I_{beam}[i] = 1353 \cdot (1 - 0.14 \cdot H) \cdot \left(0.7^{AM[i]^{0.678}}\right) + 0.14 \cdot H \quad (12)$$

$$I_{direct}[i] = I_{beam}[i] \cdot cos(\theta)[i] \tag{13}$$

$$I_{diffuse}[i] = 0.1 \cdot I_{beam}[i] \tag{14}$$

$$I_{incident}[i] = I_{direct}[i] + I_{diffuse}[i] \tag{15}$$

The total absorbed intensity of solar radiation $I_{absorbed}[i]$ is calculated at each time step, incorporating a surface absorption factor F_a, which represents the fraction of incident solar radiation absorbed by the surface. The absorption factor F_a, typically ranges from 0 to 1. Here, $F_a = 0.98$ is assumed [22].

$$I_{absorbed}[i] = F_a \cdot I_{incident}[i] \tag{16}$$

In addition, partial shading of the solar panels may significantly affect the absorbed radiation. Murugesan and Liscouët-Hanke [15] quantified the potential amount of shading on wing, tail, and fuselage with a detailed orientation analysis. The aircraft configuration (i.e., wing and tail configuration) significantly affects shading, with factors reducing absorbed radiation by 12–40%: high-wing and T-tail aircraft will have minimal shading on those surfaces. The current SPS tool includes preset values for typical aircraft configurations. A detailed shading analysis is recommended for specific configurations. In general, installing solar cells in areas shaded for over 50% of flight time (i.e., vertical tail of side panels of the fuselage) is not recommended, as the added weight will in most cases outweigh the benefits of the solar power supply. More detailed shading pattern analysis can inform solar cell segmentation, connection to arrays, and installation of bypass diodes to minimize impact on overall array power output [12,15,22].

Previous studies [14–16] assumed that aircraft operate above cloud levels, but for smaller aircraft, especially those involved in air taxi operations, flying at lower altitudes requires accounting for cloud cover in radiation calculations, even if tourism-based flight operations (such as sightseeing) are often a "good weather" operation. There is no universal cloud effect modeling in the literature; however, several papers provide experimental data for specific geographic locations or conditions. Amusan et al. [34] measured a reduction in solar cell power output of 24% for light clouds and 67% for heavy clouds for a particular day. Jiang et al. [35] provided a detailed survey of the cloudiness effect on solar power output based on meteorological measurements in China in 2012. Their study found that ice clouds reduce plane-of-array irradiance (POAI) by 10–13% and liquid water clouds reduce it by 16–22%. Collectively, all cloud types decrease POAI by more than 27%, with the most significant reduction (34%) occurring in winter. Solar cell manufacturers also note that cloud conditions can reduce output power by 75–90% [36]. Based on these findings, using a conservative approach, the conceptual design model assumes that solar panels would achieve around 25% of their normal output power under cloudy conditions. In addition, in the mission analysis, the number of sun and overcast hours in the geographical location can be defined.

2.1.2. Module 3: Improved Power Yield Analysis

Given that aircraft experience a wide range of temperatures—from as high as +55 °C on the ground to as low as −80 °C at high altitudes—the efficiency and power output model is updated to reflect these conditions.

The power generated by photovoltaic (PV) panels depends on their temperature and the solar irradiation. To determine the maximum electrical power output, we used the following calculation [37]:

$$P_m = P_{m,stc}(1 - \gamma(T_{PV} - 25))\frac{I_T}{1000} \tag{17}$$

Under typical sunlight levels of 1000 W/m^2 and a PV module temperature of 25 °C, the value P_m represents the maximum possible electrical output, while $P_{m,stc}$ is the maximum power output under standard test conditions. The term γ refers to the temperature coefficient for maximum power, indicating how temperature changes impact power output. In this setup, T_{PV} stands for the PV module temperature, and I_T is the level of solar irradiation affecting the panel [38].

In addition, the solar cell module is also subject to convective heat transfer, particularly during flight. The effect of the wind speed V_W is captured in the formula developed by Skoplaski and Palyvos [39,40] in Equation (18).

$$T_{PV} = T_a + \frac{0.32 \cdot I_T}{8.91 + 2V_W}; \quad V_W > 1 \text{ m/s} \tag{18}$$

Equation (18) considers all relevant environmental factors, such as ambient temperature T_a, wind speed V_W, and solar irradiance I_T. All these parameters affect the temperature of photovoltaic (PV) modules. The equation emphasizes the interplay between solar heating, which is influenced by solar irradiance, and the cooling effect provided by wind, where higher wind speeds enhance the transfer of heat away from the module into the surrounding environment, while the wind speed is equivalent to the aircraft speed in flight conditions. A minimum wind speed of 1 m/s must be assumed for the model to be valid, which is also a realistic scenario in ground conditions.

Heat conduction to aircraft with integral wing fuel tanks also plays a role. This aspect is not considered here. Overall, the presented model provides a more realistic insight into solar system performance during flight conditions.

2.1.3. Module 4: Solar Panel Thickness and System Weight Estimation

The SPS consists of several elements: the solar modules (cells combined together and encapsulated), the electrical components (converters and wiring), and potentially a battery. This subsection outlines the weight estimation methodology implemented in the modeling framework.

In principle, two methods exist for integrating solar cells into an aircraft surface: (1) structural integration, meaning the designing and manufacturing of aircraft surfaces with integrated solar panels; and (2) adding solar panels on top of existing aircraft surfaces. Method one, widely used for experimental aircraft, is undoubtedly more weight-efficient and minimizes the effect on aerodynamics, but it might be impractical for maintaining and replacing cells. For aircraft retrofits, i.e., for larger aircraft, method 2 has to be considered as well. Method 2 is considered a conservative approach in the presented conceptual design framework.

The weight of solar panels is estimated based on the solar panel thickness. The thickness of the solar panel depends on the materials selected. Solar cell manufacturer data sheets typically provide information on the solar cell thickness and weight. However, few details on solar cell encapsulation for aircraft applications are available in the literature.

Figure 2 presents a typical PV panel setup, consisting typically of four to five layers of different materials, according to a study from Pavlovic et al. [41] regarding the best encapsulation materials for photovoltaic panels used in racing vehicles.

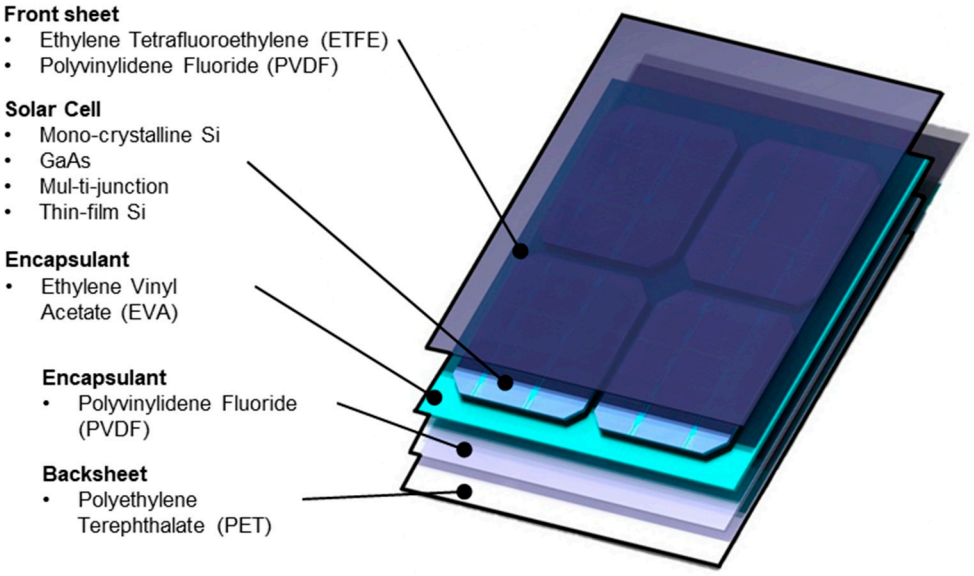

Figure 2. PV Lamination layers and potential materials, adapted from [41].

At the conceptual design level, we are interested in understanding the potential variations in thickness and weight for suitable materials. Table 1 provides a compilation of the thicknesses of various components used in solar panels, focusing on each material's minimum and maximum thicknesses. The materials analyzed, including the lamination-type layers shown in Figure 2, reveal that ETFE and PVDF exhibit the most significant variation in thickness.

Table 1. Solar panel thickness and weight analysis.

	Front Sheet		Solar Cell				Encapsulant		Back Sheet	Total Solar Panel
	ETFE [41]	PVDF [41]	Monocrystal-line Si [42]	GaAs [43]	Multi-Junc-tion [44]	Thin-Film Si [45]	EVA [41]	PVDF [41]	PET [41]	
Min. Thickness (mm)	0.28	0.08	0.165	0.14	0.14	0.15	0.02	0.08	0.2	0.44
Max. Thickness (mm)	0.28	0.5	0.165	0.175	0.14	0.18	0.2	0.5	0.2	1.58
Min. Weight (kg/m^2)	0.484	0.142	0.288	0. 8	0.84	0.15	0.019	0.142	0.27	0.581
Max. Weight (kg/m^2)	0.484	0.885	0.288	1	0.84	0.2	0.189	0.885	0.27	3.229

The configuration PVDF–thin film (a-Si)–EVA–PVDF–back sheet exhibits the highest thickness, approaching 1.6 mm. In contrast, the ETFE–GaAs–EVA–back-sheet configuration shows the lowest thickness of around 0.5 mm. The configuration PVDF–GaAs–EVA–ETFE–back sheet has a higher maximum weight, nearing 3.25 kg–m^2. In contrast, the configuration ETFE–thin film–EVA–back sheet presents the lowest weight—about 0.581 kg/m^2.

This analysis underscores the critical role of material selection in solar panel design: heavier configurations might offer enhanced durability as lighter configurations. Therefore, optimizing the material composition of solar panels is important for more detailed design phases. In this paper, focusing on understanding potential implications for early aircraft design, the data in Table 1 are used in a design of experiment (DOE).

Lastly, the thickness of the solar panels also potentially affects the aircraft's aerodynamic efficiency if mounted on top of the aircraft. A preliminary study for an NACA 64A416/4416 airfoil using computational fluid dynamics shows that with a smoothened

transition between solar panel and wing, the effect on the drag and lift is very small (0–5%). Therefore, this drag penalty and change in lift-to-drag ratio will be considered in the DOE.

The methodology for determining the wiring weight of the solar power system (SPS) is based on segmenting the solar panels according to the number of surface segments used. The total power output (watts) of the system (P_{total}) is the sum of the power generated by the solar panels on the right wing (P_{rw}), left wing (P_{lw}), fuselage (P_f), and horizontal tail (P_{ht}), expressed as:

$$P_{total} = P_{rw} + P_{lw} + P_f + P_{ht} \tag{19}$$

The estimated current for each segment is calculated separately based on the power output from the surface area of the solar panels located on the right wing, left wing, fuselage, and horizontal tail, since the voltage required by the aircraft is predetermined. The current for each segment is calculated using Equation (20):

$$I_i = \frac{P_i}{V} \tag{20}$$

where I_i is the current for segment i, P_i is the power output for segment i, and V is the voltage requirement of the aircraft. Once the current is determined, the appropriate American Wire Gauge (AWG) cable is selected based on its current-carrying capacity.

The total length of wiring required between the solar panels, charge controllers, batteries, and other electrical components is measured considering the design of the aircraft, which may necessitate long wire runs. The total wiring weight W_w is then calculated using Equation (21), with l_{rw}, l_{lw}, l_f, and l_{ht} as the wire length for the right wing, left wing, fuselage, and tail, respectively, and D_{AWG} as the unit weight of the wire per length:

$$W_w = ((l_{rw} \cdot D_{AWG}) + (l_{lw} \cdot D_{AWG}) + \left(l_f \cdot D_{AWG}\right) + (l_{ht} \cdot D_{AWG})) \cdot 2 \tag{21}$$

Following determination of the total output power of the aircraft's solar panel surfaces in watts (W), it is essential to select the appropriate converter: a DC–DC boost converter is typically required to bring the solar panel output voltage to the standard 24/28 V in the aircraft's low-voltage DC network. Typically, the converter's power rating P_{conv} is slightly higher than the peak output of the solar panels to ensure operational reliability and to account for potential power surges. A safety factor (F_S) is recommended: it allows for operational reliability and accounts for potential power surges, which aligns with general engineering practices for safety and reliability in aircraft systems, depending on the specific operational conditions and design requirements [46,47].

$$P_{conv} = P_{total} \cdot F_S \tag{22}$$

The battery sizing is essential, with a focus on optimizing battery capacity and weight to improve overall aircraft efficiency. An important step in the battery design process involves calculating the required battery capacity, denoted Q, which represents the energy storage necessary to meet the power demands of the aircraft over a specified mission profile. For aircraft missions, Q is derived by considering the total energy demand (E_{total}), depth of discharge (D), and battery efficiency (η).

The weight of the battery is a key parameter influencing aircraft performance and can be calculated using Equation (23):

$$W_{bat} = \frac{Q}{E_D} \tag{23}$$

where E_D is the battery's specific energy, typically ranging from 130–300 Wh/kg for aerospace lithium-ion batteries.

With all the abovementioned enhancements of the SPS sizing framework, conceptual designers can now perform aircraft-level trade studies for aircraft in the commuter category, considering a more realistic estimation of the SPS efficiency and weight. The framework for the aircraft-level analysis is covered in the following section.

2.2. MDAO Framework

Exploring hybrid electric aircraft concepts presents new challenges from an aircraft design perspective, especially when incorporating multiple non-traditional power sources, such as an SPS. An MDAO approach is required to evaluate the potential benefits of new technologies at the aircraft level and to perform parametric studies in the form of DOE. Here, we present an MDAO framework developed to analyze hybrid solar aircraft performance based on the approach outlined by [16] implemented within the OpenMDAO [48,49], which is shown schematically in Figure 3, as an extended design structure matrix (XDSM).

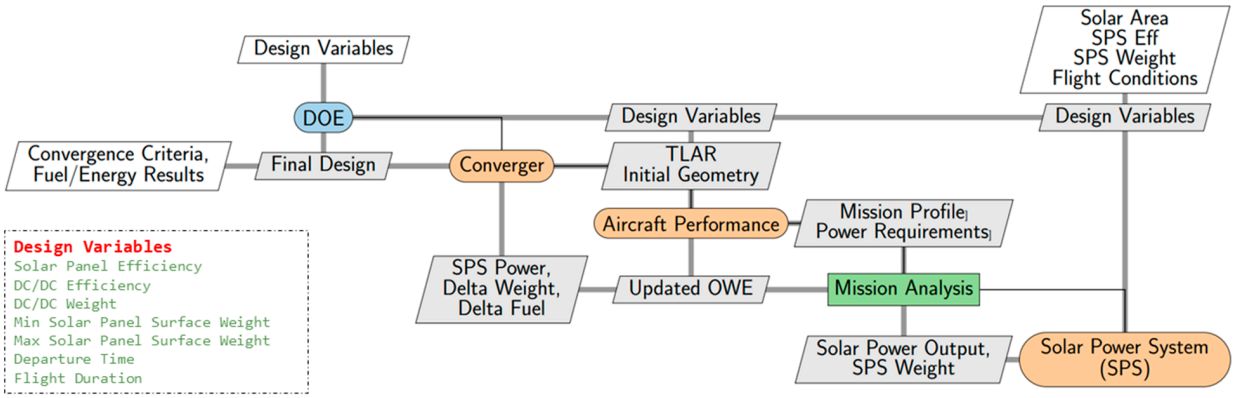

Figure 3. XDSM diagram for the MDAO workflow for aircraft-level analysis with SPS.

The DOE setup on the top of the converger uses DOE drivers facilitated within the OpenMDAO model. Initial geometry and aircraft performance are determined based on the target level of aircraft requirements (TLARs) and a mission analysis. The SPS tool calculated parameters such as SPS weight, solar power absorption at different flight conditions, and design parameters, as explained in detail in Section 2.1. This framework allows the analysis of SPS parameters such as power supply and weight and drag penalties on the aircraft's overall weight (i.e., the maximum takeoff weight (MTOW)) and fuel burn.

3. Results of the Harbour Air Case Study

This section of the paper provides an overview of the case study for the seaplane operation, followed by detailed results on the system level (SPS) and aircraft level.

3.1. Case Study Overview

Air taxi and seaplane operations for tourism provide an interesting case study for SPS implementation due to their mainly daylight and seasonal operation. Harbour Air is a Canada-based seaplane service located in Vancouver, British Columbia, providing scheduled flights and charter services along with scenic tours between major cities like Vancouver, Victoria, Nanaimo, and Seattle, among others, as well as connecting smaller communities and locations across the region. Harbour Air's operation is typical and thus representative of this type of aircraft operation. Table 2 summarizes the operational data from 2023 [41]. The scheduled services ran between April and September, and the flights were between 7:30 AM and 6:05 PM (with the exception of M3). Most of the flights had a duration of less than one hour. During this time of the year, these operation hours are mainly within daylight hours, as shown in the mission analysis in Table 2.

Table 2. Summary of typical flight schedule of Harbour Air operations [25].

Mission	Distance (km)	Duration (Average) (min)	Operating Hours (Earliest Departure–Latest Arrival)
M1: Richmond–Victoria	75	30 min	8:00 AM–4:45 PM
M2: Richmond–Sechelt	40	20 min	8:45 AM–6:00 PM
M3: Victoria–Whistler	190	135 min	7:30 AM–10:40 PM
M4: Vancouver–Powell River	105	40 min	7:50 AM–3:55 PM
M5: Vancouver–Whistler	110	45 min	9:00 AM–11:55 AM
M6: Vancouver–Tofino	190	50 min	11:30 AM–12:30 PM
M7: Vancouver–Seattle	195	55 min	12:30 AM–1:30 PM
M8: Richmond–Salt Spring	44	25 min	8:00 AM–6:05 PM
M9: Powell River–Comox	35	20 min	9:00 AM–5:00 PM

To account for operational variability in real-world scenarios, the authors analyzed all nine representative missions based on the following data. Mission routes and flight times were derived from the airline's public schedule and environmental factors, including clear and cloudy days from April to September, and were incorporated to simulate realistic weather conditions from public statistical weather data. Two operational scenarios are evaluated: (1) flight operations only, where the auxiliary SPS supplies the aircraft's essential electrical systems exclusively during flights, and (2) extended operations, where the SPS also supplies power for 30 min before and after the flight while the aircraft is parked. These considerations enhance the practical relevance of the analysis, providing a more comprehensive evaluation of the proposed system.

This paper focuses on the DHC-2 Beaver, one of the aircraft within the Harbour Air fleet, because this particular aircraft is part of the so-called eBeaver project [29]. The DHC-2 is a high-wing aircraft. Figure 4 illustrates the potential surfaces available for solar panel installation and a conceptual layout of the SPS on the DHC-2 Beaver aircraft. The aircraft operates with a DC generator driven by a Pratt & Whitney P-985 Wasp Junior engine. Each designated surface is equipped with an independent DC–DC converter to manage and transfer power from the solar panels. The SPS architecture demonstrates the flow of energy from the solar panels, encapsulated across various aircraft surfaces. After undergoing conversion via the DC–DC converters, the power is routed through electrical wiring to the aircraft's central power system. This configuration ensures a reliable supply of electrical energy to meet the operational demands of the aircraft. Tables 3 and 4 outline the key parameters of DHC-2 Beaver aircraft and the SPS parameters.

In the following case study, Section 3.2 presents the power output analysis of the solar power system (SPS), including key factors influencing performance. This is followed by Section 3.3, which provides a detailed mission analysis to evaluate the operational feasibility and energy demands. Section 3.4 outlines the SPS weight estimation, focusing on material choices and system integration implications. Finally, Section 3.5 introduces the MDAO results, with Section 3.6 detailing a DOE approach to explore design variables and performance trade-offs systematically. In Section 3.7, several hybridization strategies are explored.

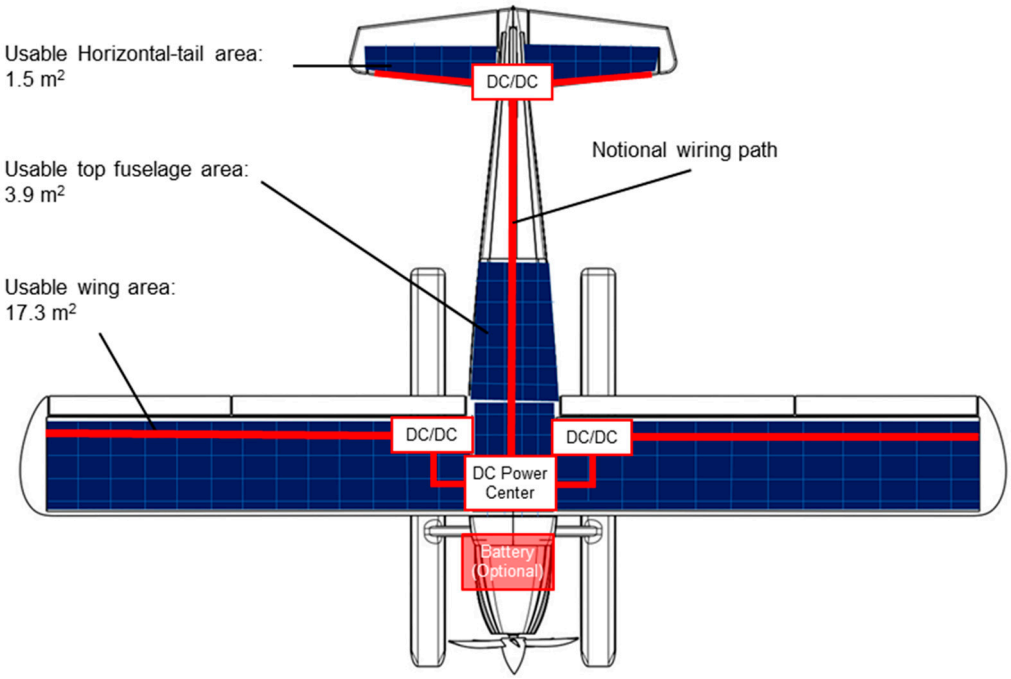

Figure 4. DHC-2 Beaver top view with potential usable surface areas for solar panels and a notional SPS layout.

Table 3. Key aircraft parameters [50].

Aircraft Parameters DHC-2	Values [unit]
Maximum Takeoff Weight	2313 kg
Operating Empty Weight	1361 kg
Payload	953 kg
Fuel Capacity	360 kg
Service Ceiling	5500 m
Endurance	3.52 h
Range	732 km
Fuel Consumption	94.5 L/h (25 U.S. gal/h)
CO_2 Emissions	0.24 kg/PAX-km
Cruise Speed	230 km/h
Stall Speed	96 km/h
Power	340 kW (450 hp)
Generator Power	~1.5 kW (28–30 DC–50 A)
Battery Capacity	24 V

Table 4. Key SPS parameters.

SPS Parameters	Values [unit]
System Voltage (V)	28–30 DC
Photovoltaic Technology	Monocrystalline silicon
Photovoltaic Cell Efficiency	25% [11]
Hybrid Powertrain Architecture	Parallel hybrid
Battery Specific Energy Density (Wh/kg)	150 [51]
Solar Cell Covering	Single-celled (PVDF–cell–EVA–PVDF–back sheet)
Converter Input Voltage	24–80 VDC [47]
Converter Output Voltage	24.3 VDC [47]
Converter Output Current	70 Amp [47]

Table 4. *Cont.*

SPS Parameters	Values [unit]
MPPT Type	Victron Energy SmartSolar MPPT Tr VE. Can 150 V 70 amp [52]
Converter Capacity	0.933 kW/kg [47]
Converter Efficiency	94% [47]
Wiring Type	AWG-8 24 Amp
Wiring Weight	0.104 kg/m [53]
Wiring Length	33 m (Figure 4)
Usable Surface Area	22.7 m^2 (Figure 4)

3.2. SPS Power Output Analysis

In the first step, the new calculation capability presented in Section 2 is used to better understand the solar panel efficiency across the flight mission for this case study. As the DHC-2 typically flies at around a maximum altitude of 5.5 km at a cruise speed of 65 m/s, one can see from Figure 5 that the solar cell efficiency ranges between 25% and 29% for a cell with manufacturers' standard conditions indicated at 25%.

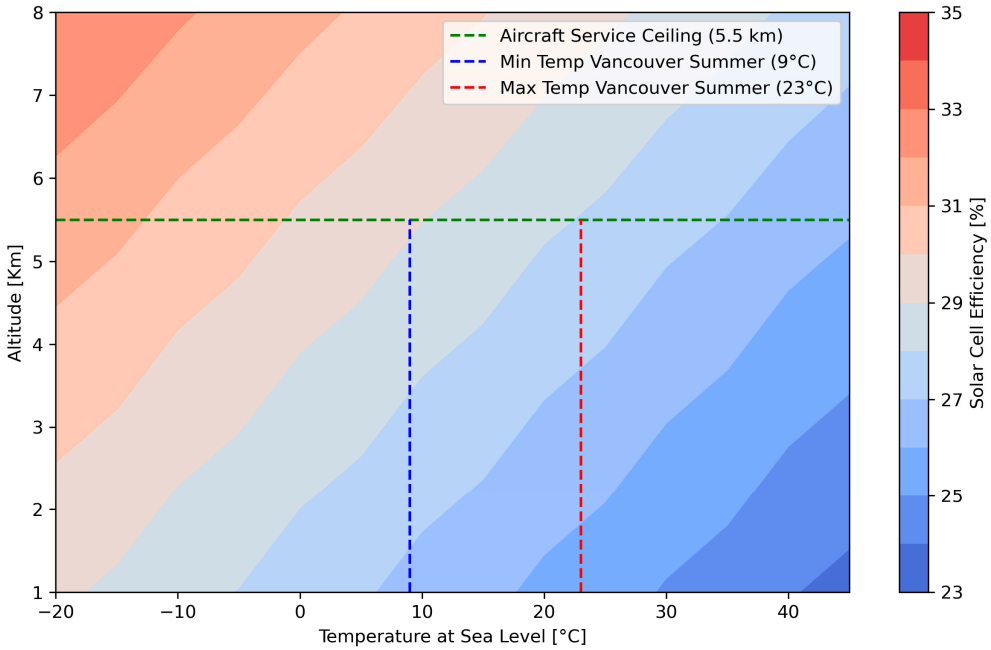

Figure 5. Contour plot of solar panel efficiency (at V = 65 m/s).

In the second step, all the missions outlined in Table 2 were analyzed according to the flight schedule indicated on the Harbour Air website. If there were several flights a day, we analyzed all the flights for the complete season. For each flight, the amount of energy absorbed by the solar panels was calculated using the framework presented in Section 2.1, which considers various parameters, including the mission's start time, day of the year, departure and arrival locations, and solar panel inputs. The power output for each mission was calculated by considering the total flight distance between two destinations, along with additional factors such as layovers during parking and return flights, according to Harbour Air's day-to-day scheduled operations.

Figure 6 provides the detailed power analysis for M1 (Richmond to Victoria) for an early morning flight in May. The graph shows the solar panel output power on the ground and during the flight mission. In addition, the generator power assumptions are shown for a realistic and conservative scenario of ground power usage. The realistic scenario assumes

no generator power usage on the ground, while the conservative scenario assumes 30 min of ground power usage before and after each flight. As the aircraft's electrical generator has a capacity of 1.5 kW, one can see that the solar output power is above this maximum power level, even for the study investigating how much excess power is available that could be used to support the propulsion system of the eBeaver. The generator is connected to the aircraft engine shaft and is typically not used on the ground. Replacing this generator with a solar power supply would provide additional ground power without emission or noise.

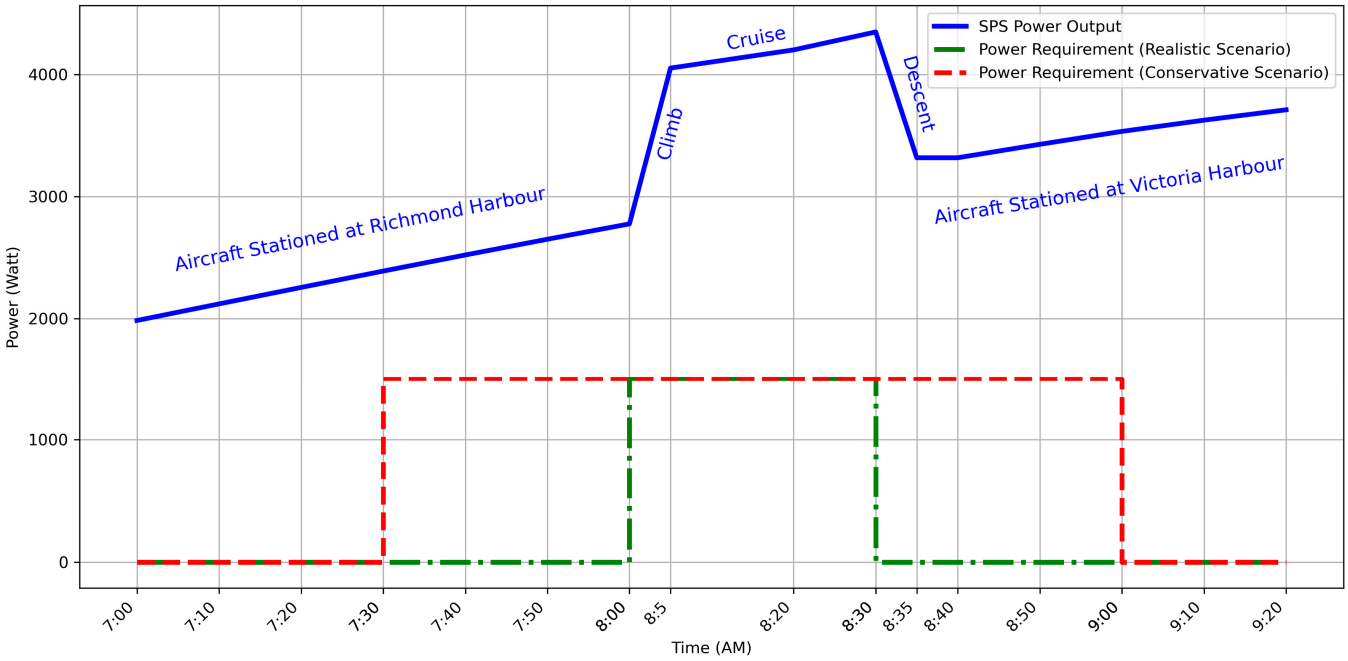

Figure 6. Generator power requirement for mission flight operation of the DHC-2 Beaver (Richmond–Victoria route—May 28) for realistic scenario (power required during flight only) and conservative scenario (power required 30 min before and after flight).

The Richmond-to-Victoria mission, with ten flight operations per day, represents the busiest route. We have selected this for a detailed analysis, depicted in Figure 7. The mission begins at 8:00 AM, with the aircraft cruising at an altitude of 5 km while maintaining a standard velocity. The plane lands at Victoria Harbour at 8:30 AM, where it remains parked at sea level, subject to the ambient conditions typical of the Victoria area. The return flight to Richmond commences at 9:00 AM, with the aircraft landing at Richmond Harbour at 9:30 AM, where it remains parked under similar sea-level and ambient conditions. This mission is repeated throughout the day according to the company's flight schedule until 6:15 PM. The analysis assesses the SPS excess power under two scenarios (realistic and conservative) across four conditions: clear and cloudy weather evaluated for May 28 and September 30.

The power analysis for the Richmond-to-Victoria mission on a clear day, represented by the blue line for May 28, indicates a substantial power surplus, with output peaking at approximately 5 kW around midday, showing the system's ability to meet and exceed the aircraft's electrical load requirements consistently. This surplus energy can be utilized to charge onboard batteries to be used to supplement propulsive power in the case of a modification of the aircraft to an electric or hybrid electric propulsion system.

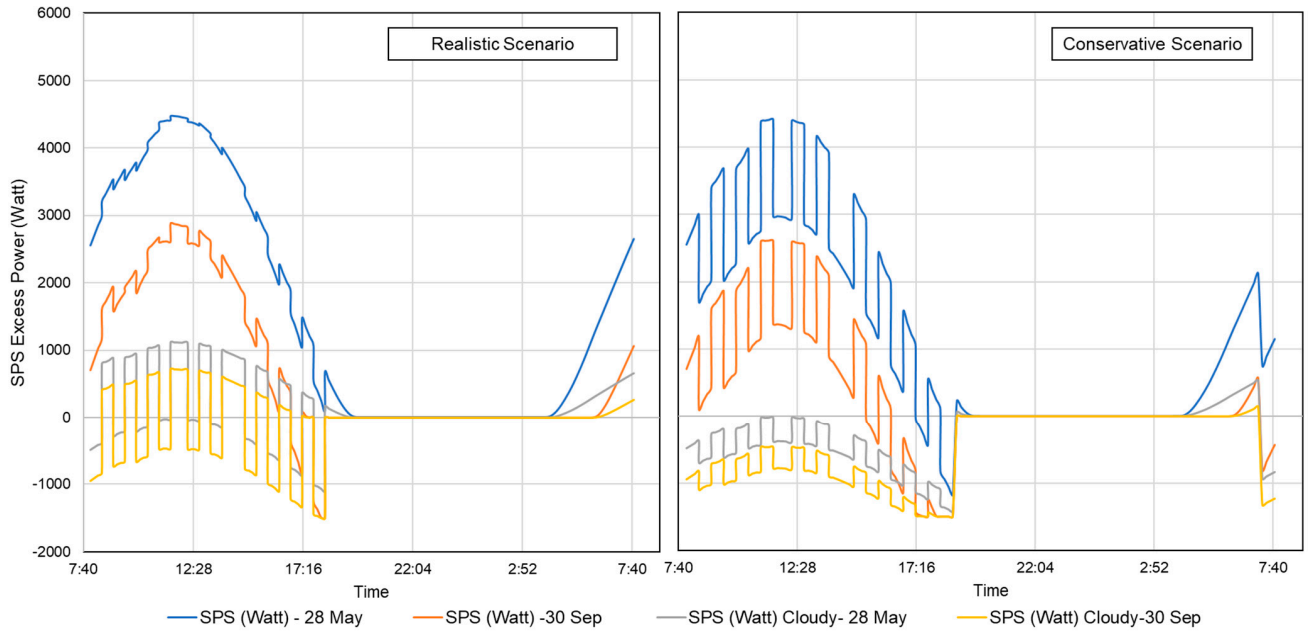

Figure 7. Generator SPS power analysis for Richmond to Victoria of 10 missions alternating between ground and flight operations on different days and under varying conditions.

Seasonal variations significantly affect the SPS's performance, as shown by the data for September 30 in Figure 7. The orange line, representing SPS output on a clear day in late September, follows a similar pattern to May 28, with a noticeable reduction in peak power levels. On this date, the SPS achieves a peak excess power of around 4 kW, reflecting reduced solar irradiance as the season transitions from summer to autumn. Despite this decrease, the SPS continues to generate sufficient excess power throughout the day, although the peak performance period is shorter.

Cloudy days substantially reduce the SPS performance, as depicted by the gray and yellow lines for May 28 and September 30, respectively, in Figure 7. On May 28, under cloudy conditions, the SPS struggled to reach a peak of 2 kW, with frequent dips below zero, indicating periods when the system failed to meet the aircraft's electrical load demands. The situation worsens on September 30, when the SPS consistently struggles to maintain positive power generation throughout the day. Cloudy conditions highlight the need for robust energy storage solutions.

In summary, the example of the M1 (Richmond to Victoria) analysis presented in Figure 7 under conservative conditions further emphasizes the seasonal and weather-related variations in SPS performance. On clear days, peak excess power reaches approximately 4 kW in May and 3 kW in September. However, cloudy conditions reduce these peaks to 1 kW in May and 0.5 kW in September. Obviously, during operations close to or past sunset, the SPS excess power drops below zero across all conditions. These findings underline the importance of supplementary power sources to accommodate the variability in solar energy generation and ensure reliable aircraft operations under varying environmental conditions. In the following, a summary of a similar analysis is presented for all missions of the Harbour Air schedule.

3.3. SPS Excess Energy Analysis

Figure 8 summarizes the surplus energy (measured in kWh) generated during flights on various routes presented in Table 2, accounting for differing weather conditions and dates. This segmentation offers a detailed exploration of how seasonal variations and meteorological conditions influence solar energy generation.

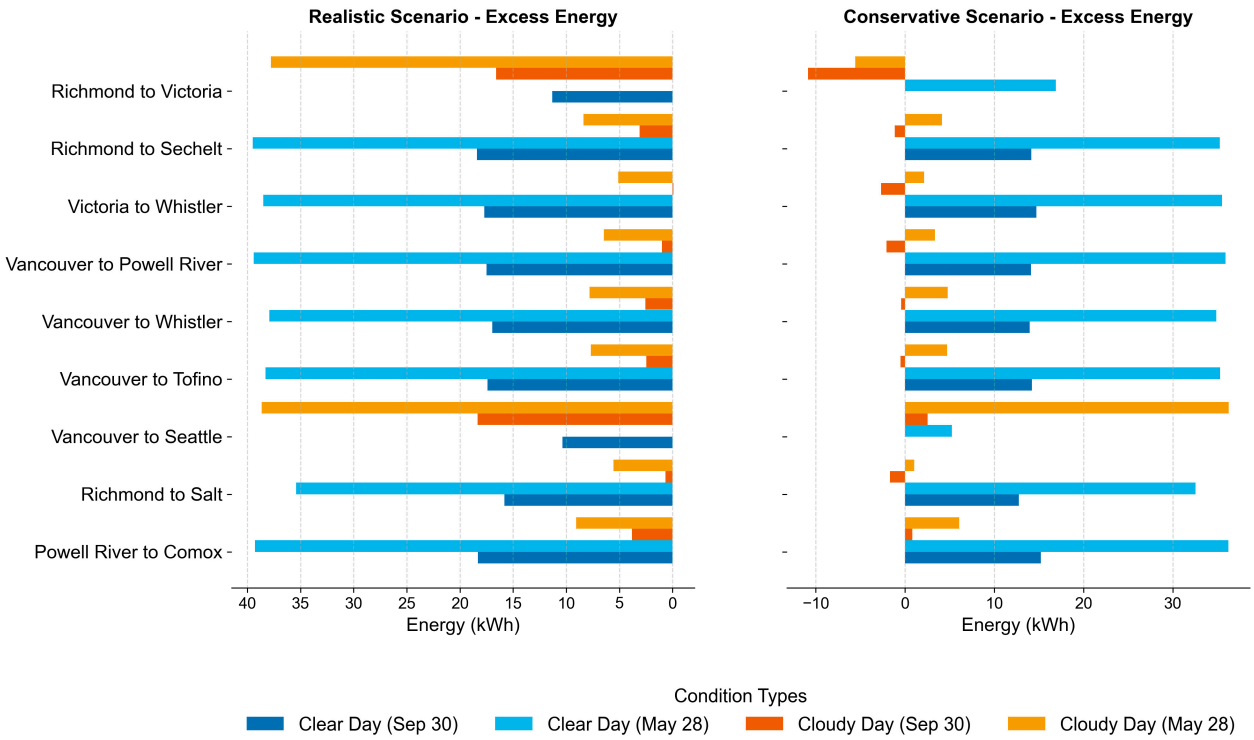

Figure 8. Excess energy analysis for realistic and conservative scenarios: evaluation of 9 mission routes alternating between ground and flight operations on different days under varying conditions.

Under clear weather conditions on May 28, SPS performance reached its peak efficiency, with routes such as Vancouver to Powell River and Victoria to Whistler generating up to 40 kWh of surplus energy, thanks to the favorable influence of the high solar irradiance and extended daylight hours characteristic of late spring. However, during cloudy conditions and autumn operations on September 30, reduced solar irradiance and shorter daylight resulted in significantly diminished energy generation, occasionally leading to deficits under conservative scenarios. One can see that for the realistic scenario (no ground electrical power consumption), all missions show a positive excess energy balance. Only two missions (M1 and M8) show a negative balance for the cloudy day scenarios for a conservative approach.

There are several paths to solve this issue, as follows.

1. Size a battery to cover all these power demands. However, this means that the aircraft with an SPS would need to carry a battery that was only required on a few occasions during a season; hence, the battery should be optional.
2. Carry out this mission with an aircraft without an SPS (or with this optional battery).

Overall, the impact of battery sizing on the system weight and the impact of associated aircraft performance is further analyzed in subsequent sections.

3.4. SPS Weight Overview

The weight analysis chart in Figure 9 illustrates the impact of installing monocrystalline silicone solar panels on the DHC-2 Beaver aircraft. The solar cells' weight is 0.228 kg/m^2. However, the overall weight varies significantly due to the encapsulation material, which ranges between 0.58 kg/m^2 and 3.23 kg/m^2. This variability in encapsulation materials impacts the total weight of the solar power system across different surfaces.

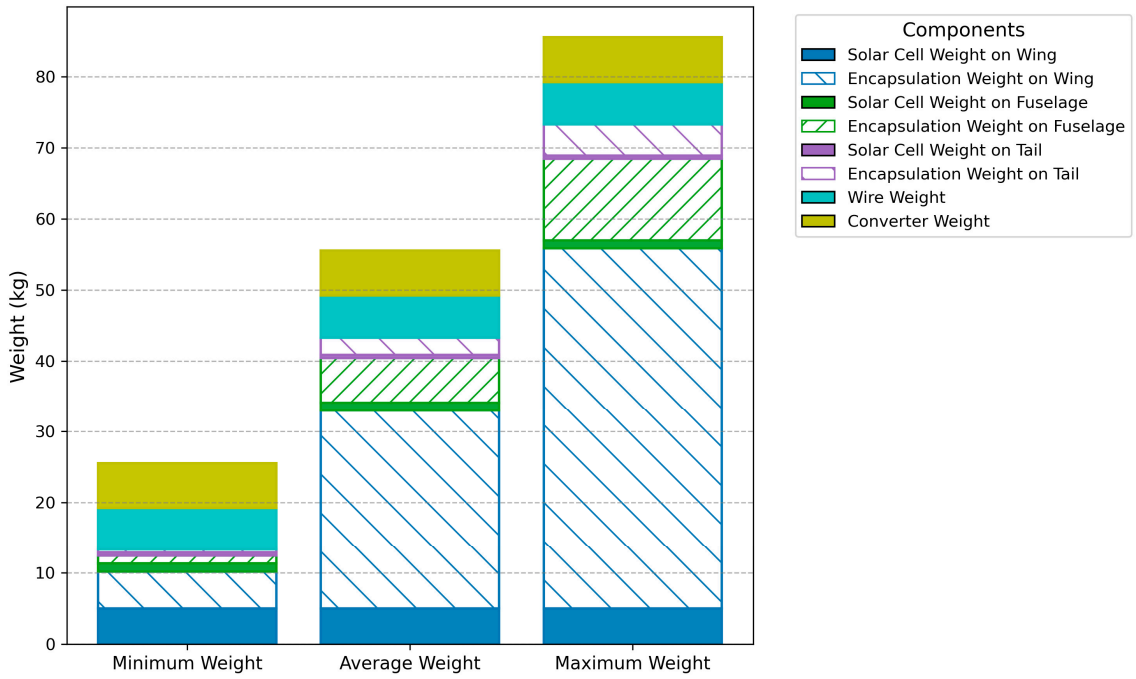

Figure 9. SPS weight analysis for DHC-2 Beaver aircraft, assuming monocrystalline (Si) solar cells.

The figure illustrates the range of minimum to maximum weight contributions of the SPS on various aircraft surfaces, such as the wing, fuselage, and tail. It emphasizes the importance of material selection in encapsulation to achieve an optimal balance between weight and performance. One can see that the majority of the weight uncertainty is due to the system installation and encapsulation. Overall, the system weight without a battery can vary between around 25 kg to 85 kg if all surfaces indicated in Figure 4 are covered.

3.5. MDAO Analysis

With detailed information on the SPS power output and weight, one can now analyze the aircraft-level impacts. Figure 10 illustrates the mission profile of the DHC-2 Beaver aircraft for Vancouver to Powell River, highlighting altitude and power requirements throughout the flight phases. Power demand peaks during takeoff and climb, then decreases during cruise. As the aircraft descends, power further reduces, continuing to drop before landing.

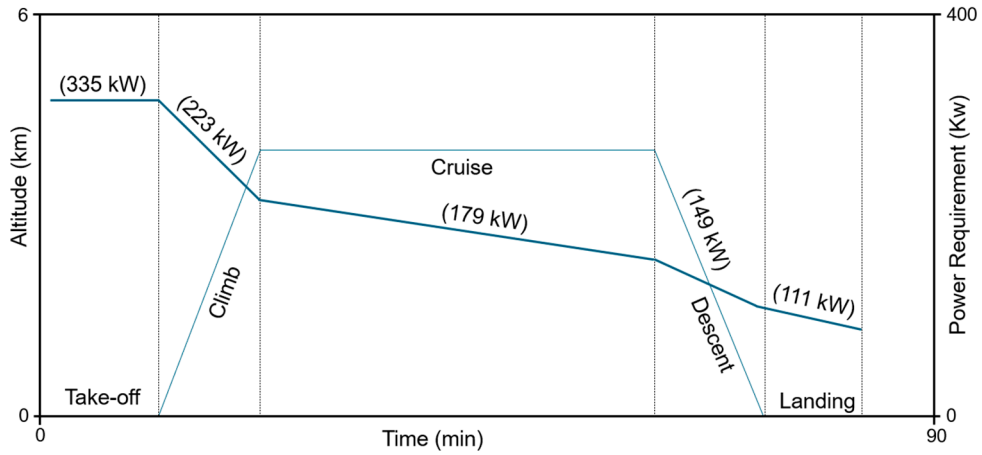

Figure 10. Mission profile: altitude vs time with power requirements for the Beaver aircraft baseline mission.

The MDAO framework presented in Section 2.2 is used to analyze how much power the SPS can generate and its impact on fuel savings and overall aircraft performance. The fuel burn comparison in Figure 11 shows the fuel consumption differences between the DHC-2 Beaver aircraft and SPS-integrated configurations. During all flight segments, specifically in the cruise segment, the SPS integration offers a reasonable decrease in fuel burn over the conventional Beaver.

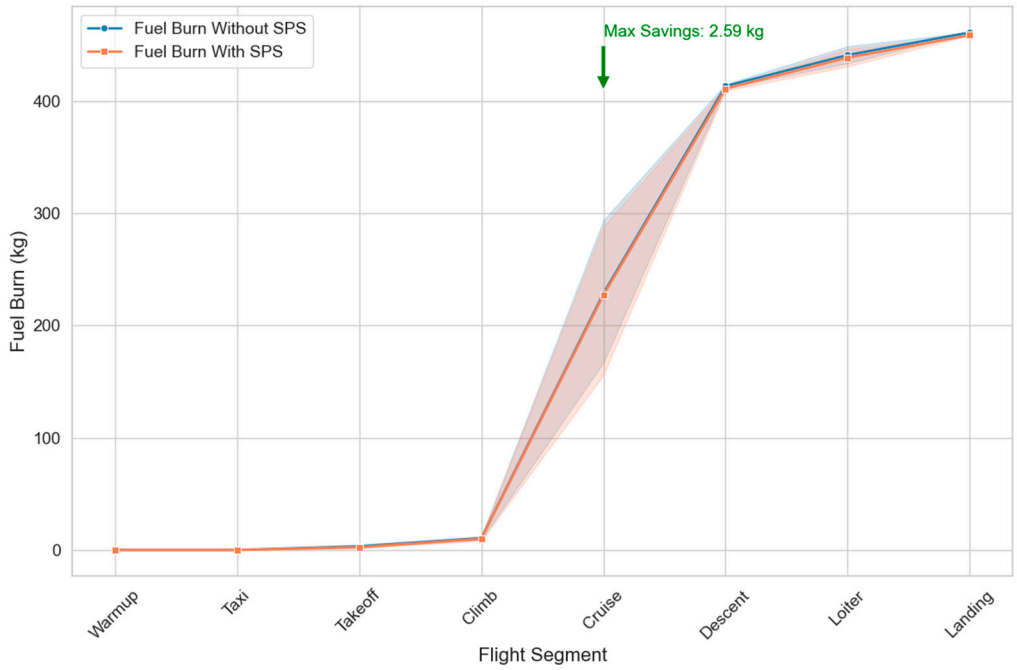

Figure 11. Fuel burn comparison.

To coordinate the insights from multidisciplinary analysis, we now employ a DOE approach to explore the sensitivity of SPS performance to key parameters. While the SPS analysis provides a comprehensive view of how the SPS impacts fuel consumption and overall performance, the MDAO-DOE methodology enables systematic evaluation of environmental, technological, and mission variables to understand their effects on aircraft performance better.

3.6. DOE Analysis

The performance of SPS is highly dependent on environmental factors (e.g., solar irradiance, cloudiness), technological parameters (e.g., panel and DC–DC efficiency and weights), and mission parameters (e.g., flight duration, altitude, time of the day). These variables can lead to significant variations between performance estimates during conceptual sizing and outcomes from detailed mission analysis. Therefore, the sensitivity of this system to variables must be explored. SPS integration with aircraft performance uses an iterative process, and design variables such as solar panel and DC–DC efficiency, absorptance, and panel area are analyzed through the DOE, influencing key parameters such as MTOW, SPS weight and energy, and fuel burn.

Table 5 summarizes the DOE parameters and Figure 12 summarizes the effect of design parameters on delta fuel burn for hybrid solar power systems.

Table 5. Parameters for the design of experiments.

Parameter [Unit]	Value Range [min–max]
Solar cell efficiency (%)	20–50
Solar cell surface weight (kg/m^2)	0.60–0.871
DC–DC converter efficiency (%)	0.9–0.98
Specific power of the battery (Wh/kg)	250–300
Cruise altitude (m)	2000–6000

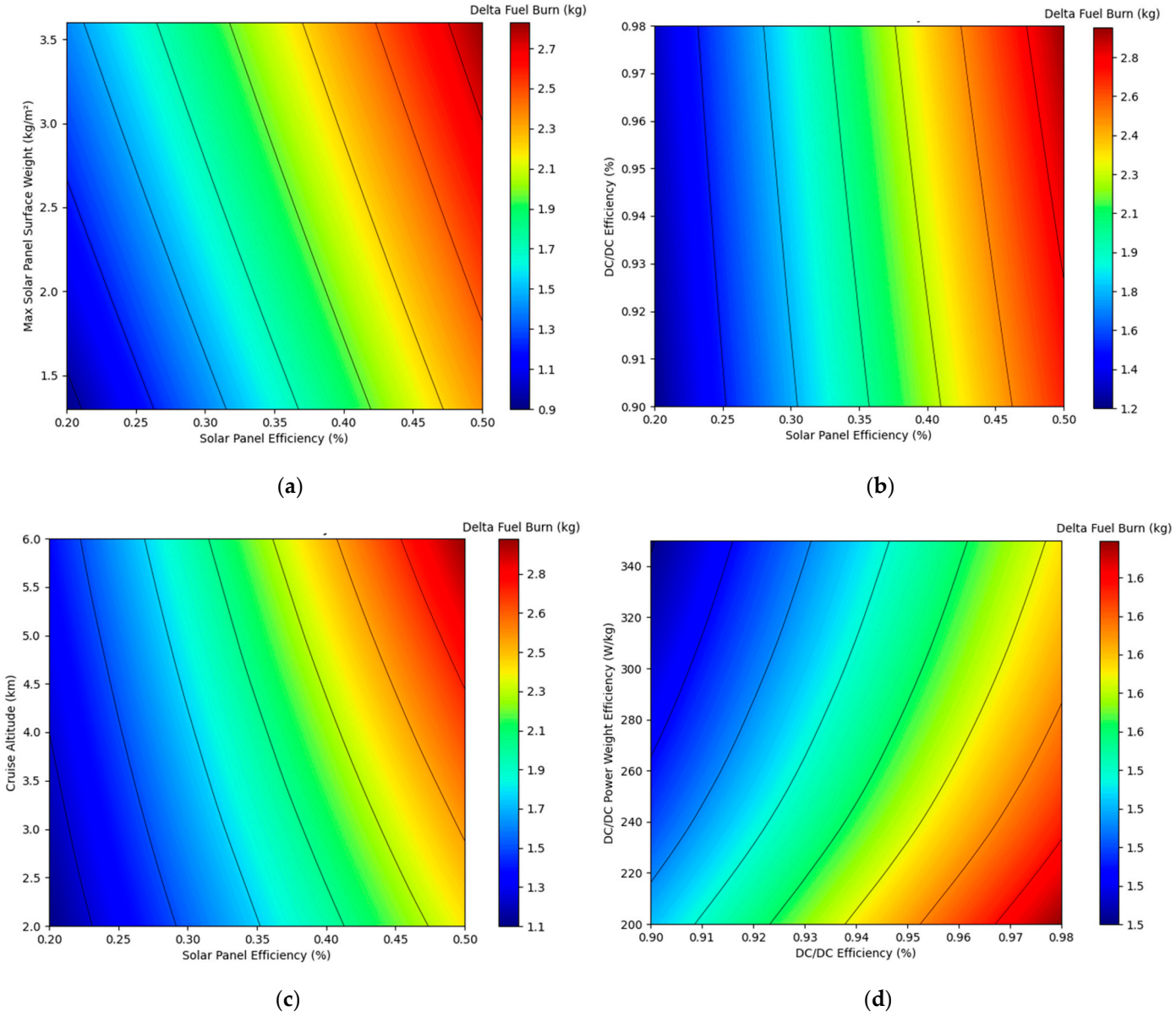

Figure 12. Delta fuel burn for (**a**) solar panel efficiency and max solar panel surface weight, (**b**) solar panel efficiency and DC–DC efficiency, (**c**) solar panel efficiency and cruise altitude, and (**d**) DC–DC efficiency and DC–DC power weight efficiency.

As solar panel efficiency increases from 20% to 50%, there is a marked decrease in fuel burn across all values of surface weight, with higher efficiency achieving the maximum savings. Increased solar efficiency correlates with 1 to 3 kg fuel burn reduction with solar panel weight, DC–DC efficiency, and cruise altitude. Increasing the surface weight from

1.5 to 3.5 kg/m^2 has a lesser effect, but still contributes to fuel savings. For solar panel efficiency plotted against DC–DC efficiency, the color gradient suggests that small gains in DC–DC efficiency, especially when solar efficiency is also high, can implicitly enhance fuel savings. Additionally, operating at higher altitudes (up to 6 km) further improves fuel savings due to increased solar irradiance and reduced atmospheric drag.

Figure 12a shows the effect of solar panel efficiency on various outputs, such as MTOW, fuel mass, and battery mass. Increasing DC–DC efficiency reduces fuel mass by improving power transfer efficiency and lowering fuel load requirements. MTOW decreases slightly with higher DC–DC efficiency, while battery mass remains largely unaffected, indicating its dependence on other factors. Appendix A shows Figure A1, which focuses on DC–DC efficiency and its relationship with the outputs. Increasing DC–DC efficiency reduces fuel mass, reflecting improved power transfer efficiency. MTOW decreases slightly, while battery mass shows minimal variation, indicating its dependence on other factors. Similarly, Figure A2 outlines the effect of solar panel surface weight on the outputs, and it largely shows that increasing panel weight leads to an increase in MTOW due to the added weight of solar panels. This trade-off is expected as heavier solar panels contribute to the structural load.

Overall, the DOE results highlight that solar panel and DC–DC converter efficiency, panel weight, and cruise altitude significantly affect SPS performance. Increasing solar panel efficiency from 20% to 50% can reduce fuel burn by 1–3 kg per mission, with higher cruise altitudes further enhancing savings due to increased solar irradiance and reduced drag. While individual mission fuel savings are modest (2–4%), the cumulative impact across a fleet is substantial, with the Richmond-to-Victoria route alone achieving daily CO_2 emissions reductions of 94.8 kg or 34.6 metric tons annually. Expanding SPS use and improving solar panel efficiency amplify these benefits while providing zero-emission power for ground operations during sunny conditions.

Figure 13 presents a pair plot analysis examining the relationships between design and response variables in integrating an SPS with aircraft performance. This analysis highlights critical factors influencing SPS performance, which include solar panel efficiency, DC–DC converter efficiency, panel weight, and cruise altitude. The diagonal portions of the pair plot show varying distributions, revealing each variable's stability. For instance, a larger or multi-peaked distribution in variables like battery weight indicates that the variable may represent several distinct designs or operational conditions. These robust connections are essential for matching the importance of optimizing these variables to achieve reliable and efficient SPS integration. These findings underline the importance of optimizing these variables to achieve reliable and efficient SPS integration.

3.7. Aircraft Power Hybridization Using the SPS

In the following, we examine two configurations: direct solar power utilization without battery storage (SPS without battery) and battery hybridization, where the excess solar power is stored and used in parallel with conventional fuel. The hybridization coefficients quantify the contribution of energy and power from both sources. The hybridization of energy is calculated as the ratio of total battery energy to the sum of battery and fuel energy, while the hybridization of power is derived from the ratio of electric motor power to the combined power of the internal combustion engine and electric motor. Additionally, parameters such as energy and power requirements are evaluated to size the battery appropriately.

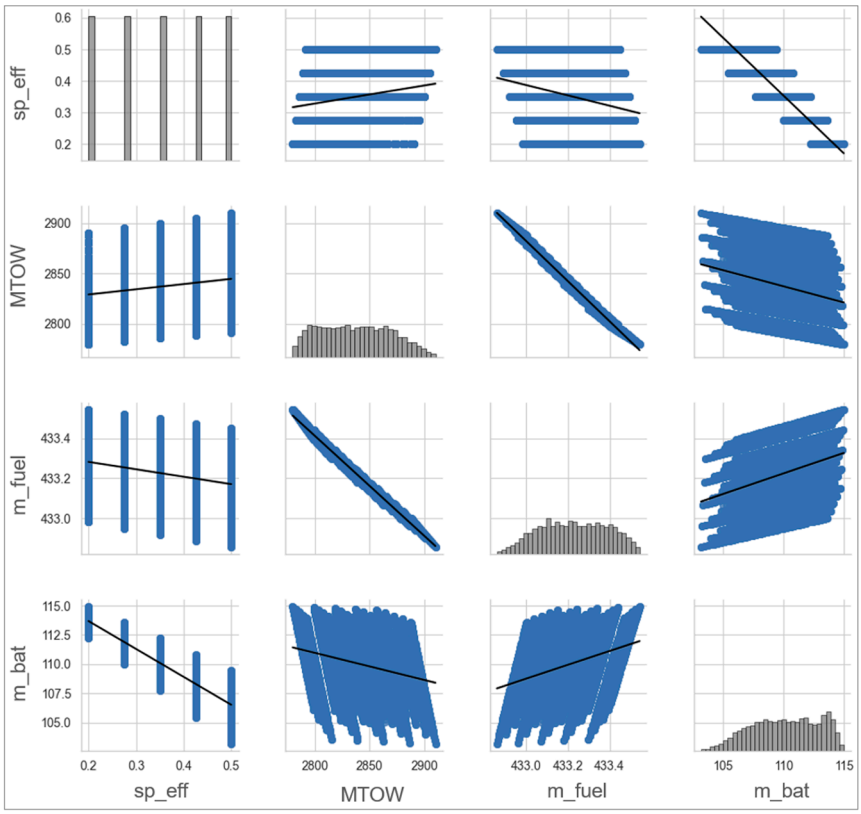

Figure 13. Pair plot of design and response variables for SPS-aircraft integration with sp_eff design variable.

Table 6 summarizes the results of the analysis and shows that hybridization and SPS integration improve DHC-2 Beaver fuel burn, battery weight, and MTOW. In the baseline (conventional) designs, progressive hybridization levels (HP = 0.05, 0.07, and 0.1) reduce fuel burn, but increase MTOW due to battery weight. This shows that hybridization alone improves fuel efficiency. Integrating the solar power system decreases fuel consumption to 459 kg and increases MTOW by 69 kg (average scenario) in the SPS-only configuration, demonstrating solar power's fuel efficiency potential without batteries. Finally, combined SPS and hybridization configurations show the cumulative benefits of solar and hybrid technologies. SPS with HP = 0.1 has the lowest fuel burn of 421 kg, and the battery weight has also been reduced. The table shows that hybrid and solar technologies reduce fuel consumption and maximize performance by balancing fuel savings with MTOW increases.

Table 6. Effects of hybridization and SPS on DHC-2 Beaver fuel burn, battery weight, and MTOW.

Run Configuration	Fuel Burn (kg)	Battery Weight (kg)	MTOW (kg)	Battery Added (kg)	MTOW Increase (kg)
Baseline (Conventional, No Battery)	461	0	2622	-	-
Baseline (Conventional Cruise HP = 0.05)	441	84	2687	84	65
Baseline (Conventional Cruise HP = 0.07)	433	118	2713	118	91
Baseline (Conventional Cruise HP = 0.1)	422	169	2752	169	130
SPS Only (No Hybridization)	459	0	2745	69 (SPS)	123
SPS + Cruise (HP = 0.05)	439	76	2804	76 + 69 (SPS)	182
SPS + Cruise (HP = 0.07)	432	110	2830	110 + 69 (SPS)	208
SPS + Cruise (HP = 0.1)	421	161	2869	161 + 69 (SPS)	124

Table 6 shows that an additional SPS has the potential to reduce aircraft mission fuel burn; however, since the present system is not optimized, the actual fuel burn reduction could be even higher. The SPS may reduce structural weight and improve fuel efficiency if the aircraft were resized and designed to lower MTOW. A fully optimized design could enhance the benefits of SPS and hybrid technologies, reducing fuel consumption and improving aircraft performance. In addition, the overall SPS area required could also be optimized.

4. Conclusions

This paper examined the integration of solar power systems as a retrofit to conventional and hybrid electric seaplane operations, using a comprehensive multidisciplinary design analysis and optimization framework that has been enhanced to capture specific operation scenarios of smaller, low-flying aircraft and features a more detailed weight estimation, i.e., for the encapsulation weight. A detailed and realistic case study for the operation of Harbour Air shows that in 86% of the missions, the electrical power demand of the subsystems could be supplied by the SPS, with significant excess power that can be stored in a battery to cover alternative functions, such as zero-emission power for ground operations. Hence, a retrofit of old aircraft, such as the Beaver, with an SPS has the potential to reduce CO_2 emissions: modest savings with current technologies up to significant savings for incremental increase in SPS performance or combination with an electric or hybrid electric propulsion.

In summary, the presented MDAO framework for aircraft with SPS, together with a realistic case study, allows the identification of potential application cases for SPS, and to find an optimized solution for a potential retrofit system. Also, it highlights that the encapsulation concept maturation requires specific attention, as it constitutes the biggest weight uncertainty in the system. This paper highlights SPS as a potential solution for reducing aviation's environmental impact and advancing sustainable air transportation.

Author Contributions: Conceptualization, S.L.-H. and M.B.; methodology, S.L.-H., M.M. and M.B.; formal analysis, M.M. and M.B.; investigation, M.M.; resources, S.L.-H. and M.M.; writing—original draft preparation, S.L.-H., M.M. and M.B.; writing—review and editing, M.M., M.B. and S.L.-H.; visualization, S.L.-H., M.M. and M.B.; supervision, S.L.-H.; project administration, S.L.-H.; funding acquisition, S.L.-H. All authors have read and agreed to the published version of the manuscript.

Funding: This research was supported by the Natural Sciences and Engineering Research Council of Canada (NSERC) Discovery Grant program under grant RGPIN-2019-05515.

Data Availability Statement: The data supporting the findings of this study are available upon request. For further information or to access the data, please contact us via email.

Acknowledgments: The authors would like to acknowledge the contributions of Greg Woods from Concordia University for his collaboration in the MDAO analysis.

Conflicts of Interest: The authors declare no conflicts of interest. The funders had no role in the design of the study; in the collection, analyses, or interpretation of data; in the writing of the manuscript; or in the decision to publish the results.

Appendix A

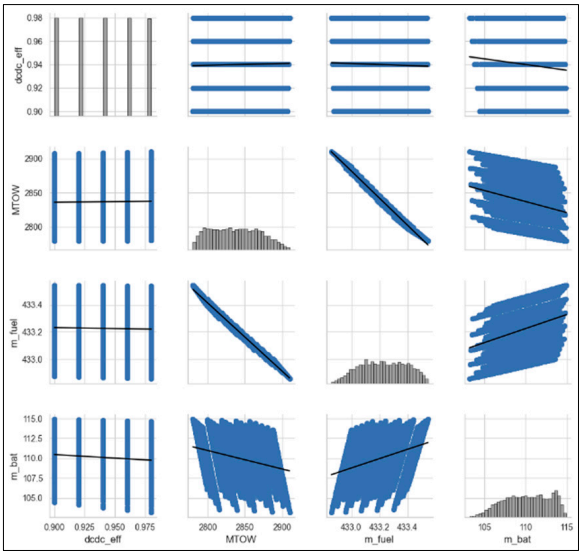

Figure A1. Pair plot of design and response variables for SPS-aircraft integration with dcdc_eff design variable.

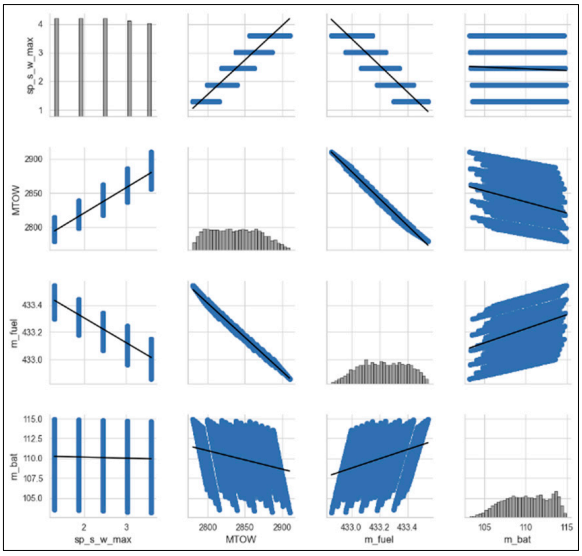

Figure A2. Pair plot of design and response variables for SPS-aircraft integration with sps_w_max design variable.

References

1. Brelje, B.J.; Martins, J.R.R.A. Electric, Hybrid, and Turboelectric Fixed-Wing Aircraft: A Review of Concepts, Models, and Design Approaches. *Prog. Aerosp. Sci.* **2019**, *104*, 1–19. [CrossRef]
2. Adler, E.J.; Martins, J.R.R.A. Hydrogen-Powered Aircraft: Fundamental Concepts, Key Technologies, and Environmental Impacts. *Prog. Aerosp. Sci.* **2023**, *141*, 100922. [CrossRef]
3. Boucher, R.J. History of Solar Flight. In Proceedings of the AIAA/SAE/ASEE 20th Joint Propulsion Conference, Cincinnati, OH, USA, 11–13 June 1984.
4. Abbe, G.; Smith, H. Technological Development Trends in Solar-Powered Aircraft Systems. *Renew. Sustain. Energy Rev.* **2016**, *60*, 770–783. [CrossRef]
5. Papis, K.; Figaj, R.; Kuś, J.; Żołądek, M.; Zając, M. Application of Photovoltaic Cells as a Source of Energy in Unmanned Aerial Vehicle (UAV)—Case Study. *E3S Web Conf.* **2020**, *173*, 02002. [CrossRef]
6. Cipolla, V.; Dine, A.; Viti, A.; Binante, V. MDAO and Aeroelastic Analyses of Small Solar-Powered UAVs with Box-Wing and Tandem-Wing Architectures. *Aerospace* **2023**, *10*, 105. [CrossRef]

7. Liu, Y.; Sun, K.; Xu, Z.; Lv, M. Energy Efficiency Assessment of Photovoltaic Array on the Stratospheric Airship under Partial Shading Conditions. *Appl. Energy* **2022**, *325*, 119898. [CrossRef]
8. Buckley, H.P.; Holt, N.; Leinonen, A.; Fournier, S.; Zingg, D.W. Preliminary Design of a Solar-Powered Hybrid Airship. *J. Aircr.* **2020**, *57*, 256–267. [CrossRef]
9. Westbrook, T.; Rostvik, H. Solar Energy and Battery Development for Unmanned Aerial Vehicles: Leading to Increased Proliferation? *Salus J.* **2023**, *6*, 59–77. Available online: https://view.salusjournal.com/index.php/salusjournal/article/view/91 (accessed on 18 February 2025).
10. Solar Impulse. Available online: https://aroundtheworld.solarimpulse.com/ (accessed on 11 January 2025).
11. National Renewable Energy Laboratory. Best Research-Cell Efficiencies. Available online: https://www.nrel.gov/index.html (accessed on 20 April 2023).
12. Liscouët-Hanke, S.; Sadaka, N.; El Chaar, R. A Supplemental Solar Power System for Future Aircraft: Challenges and Opportunities. In *The Future of Solar Power*; Nova Science Publishers: Hauppauge, NY, USA, 2023.
13. Ramírez-Díaz, G.; Nadal-Mora, V.; Piechocki, J. Descriptive Analysis of Viability of Fuel Saving in Commercial Aircraft through the Application of Photovoltaic Cells. *Renew. Sustain. Energy Rev.* **2015**, *51*, 138–152. [CrossRef]
14. Liscouët-Hanke, S.; Shafiei, A.; Lopes, L.; Williamson, S. Proof-of-Concept Analysis of a Supplemental Solar Power System for Aircraft. *Aircr. Eng. Aerosp. Technol.* **2018**, *90*, 1295–1304. [CrossRef]
15. Liscouët-Hanke, S.; Murugesan, E.S. Conceptual Design Framework for an Aircraft Auxiliary Photovoltaic System. In Proceedings of the 2018 Aviation Technology, Integration, and Operations Conference, Atlanta, GA, USA, 25–29 June 2018; American Institute of Aeronautics and Astronautics: Reston, VA, USA, 2018.
16. Licheva, G.; Mohan, V.; Jeyaraj, A.K.; Bamrah, P.; Mir, M.; Liscouet-Hanke, S. System Integration Study for a Hybrid-Electric Commuter Aircraft Concept with a Solar Auxiliary Power System. In Proceedings of the AIAA SCITECH 2024 Forum, Orlando, FL, USA, 8–12 January 2024; American Institute of Aeronautics and Astronautics: Reston, VA, USA, 2024.
17. Sun, K.W.; Ni, M. Feasibility Analysis of Hybrid Power System Used on Solar-Powered Aircraft. *Adv. Mater. Res.* **2013**, *860–863*, 118–123. [CrossRef]
18. Haws, T.; Bowman, W. Thermal Analysis of the Pathfinder Aircraft. In Proceedings of the 37th Aerospace Sciences Meeting and Exhibit, Reno, NV, USA, 11–14 January 1999; American Institute of Aeronautics and Astronautics: Reston, VA, USA, 1999.
19. Fazelpour, F.; Vafaeipour, M.; Rahbari, O.; Shirmohammadi, R. Considerable Parameters of Using PV Cells for Solar-Powered Aircrafts. *Renew. Sustain. Energy Rev.* **2013**, *22*, 81–91. [CrossRef]
20. Noth, A.; Siegwart, R.; Engel, W. Design of Solar Powered Airplanes for Continuous Flight. Doctoral Dissertation, ETH Zurich, Zürich, Switzerland, 2006.
21. Dai, Q.; Fang, X. A Simple Model to Predict Solar Radiation under Clear Sky Conditions. *Adv. Space Res.* **2014**, *53*, 1239–1245. [CrossRef]
22. Murugesan, E.S. Conceptual Design Analysis for an Aircraft Auxiliary Photovoltaic System. Master's Thesis, Concordia University, Montreal, QC, Canada, 2018.
23. Li, X.; Fang, X.; Dai, Q. Research on Thermal Characteristics of Photovoltaic Array of Stratospheric Airship. *J. Aircr.* **2011**, *48*, 1380–1386. [CrossRef]
24. Iliopoulou, C.; Kepaptsoglou, K.; Karlaftis, M.G. Route Planning for a Seaplane Service: The Case of the Greek Islands. *Comput. Oper. Res.* **2015**, *59*, 66–77. [CrossRef]
25. Harbour Air. Available online: https://harbourair.com/flight-info/flight/schedules/ (accessed on 11 July 2019).
26. Xiao, T.; Qin, N.; Lu, Z.; Sun, X.; Tong, M.; Wang, Z. Development of a Smoothed Particle Hydrodynamics Method and Its Application to Aircraft Ditching Simulations. *Aerosp. Sci. Technol.* **2017**, *66*, 28–43. [CrossRef]
27. Duan, X.; Sun, W.; Chen, C.; Wei, M.; Yang, Y. Numerical Investigation of the Porpoising Motion of a Seaplane Planing on Water with High Speeds. *Aerosp. Sci. Technol.* **2019**, *84*, 980–994. [CrossRef]
28. *Methods and Applications for Modeling and Simulation of Complex Systems: 21st Asia Simulation Conference, AsiaSim 2022, Changsha, China, December 9–11, 2022, Proceedings, Part I*; Fan, W., Zhang, L., Li, N., Song, X., Eds.; Communications in Computer and Information Science; Springer Nature: Singapore, 2022; Volume 1712, ISBN 978-981-19919-7-4.
29. Skies Mag. Harbour Air Signs First eBeaver Sales Agreement. Available online: https://skiesmag.com/news/harbour-air-signs-first-ebeaver-sales-agreement/ (accessed on 11 January 2025).
30. Bakirci, K. General Models for Optimum Tilt Angles of Solar Panels: Turkey Case Study. *Renew. Sustain. Energy Rev.* **2012**, *16*, 6149–6159. [CrossRef]
31. El Mghouchi, Y.; El Bouardi, A.; Choulli, Z.; Ajzoul, T. Models for Obtaining the Daily Direct, Diffuse and Global Solar Radiations. *Renew. Sustain. Energy Rev.* **2016**, *56*, 87–99. [CrossRef]
32. Kasten, F.; Young, A.T. Revised Optical Air Mass Tables and Approximation Formula. *Appl. Opt.* **1989**, *28*, 4735. [CrossRef] [PubMed]

33. Rihacek, J.; Sarbort, M.; Hornik, P.; Mrna, L. Solar Absorbers with a Structured Surface. *MM Sci. J.* **2018**, *2018*, 2390–2396. [CrossRef]
34. Amusan, J.A.; Otokunefor, E.B. The Effect of Cloud on the Output Performance of a Solar Module. *Int. J. Eng. Sci.* **2019**, *9*, 19665.
35. Jiang, Y.; Yi, B. An Assessment of the Influences of Clouds on the Solar Photovoltaic Potential over China. *Remote Sens.* **2023**, *15*, 258. [CrossRef]
36. Sendy, A. Do Solar Panels Work on Cloudy Days or at Night? Available online: https://www.solarreviews.com/blog/do-solar-panels-work-on-cloudy-days-or-at-night#:~:text=Yes,%20solar%20panels%20do%20work,thick%20the%20cloud%20cover%20is (accessed on 11 January 2025).
37. Pantic, L.S.; Pavlović, T.M.; Milosavljević, D.D.; Radonjic, I.S.; Radovic, M.K.; Sazhko, G. The Assessment of Different Models to Predict Solar Module Temperature, Output Power and Efficiency for Nis, Serbia. *Energy* **2016**, *109*, 38–48. [CrossRef]
38. Sun, V.; Asanakham, A.; Deethayat, T.; Kiatsiriroat, T. A New Method for Evaluating Nominal Operating Cell Temperature (NOCT) of Unglazed Photovoltaic Thermal Module. *Energy Rep.* **2020**, *6*, 1029–1042. [CrossRef]
39. Hasan, A.; Sarwar, J.; Alnoman, H.; Abdelbaqi, S. Yearly Energy Performance of a Photovoltaic-Phase Change Material (PV-PCM) System in Hot Climate. *Sol. Energy* **2017**, *146*, 417–429. [CrossRef]
40. Skoplaki, E.; Palyvos, J.A. Operating Temperature of Photovoltaic Modules: A Survey of Pertinent Correlations. *Renew. Energy* **2009**, *34*, 23–29. [CrossRef]
41. Pavlovic, A.; Mikhnych, V.; Bertoldi, M.; Fragassa, C. Investigating Encapsulation Design Strategy of Photovoltaic Cells in the Case of a Solar Race Car. *IOP Conf. Ser. Mater. Sci. Eng.* **2022**, *1214*, 012042. [CrossRef]
42. SunPower Corporation. C60 Solar Cell—Mono Crystalline Silicon. Available online: http://eshop.terms.eu/_data/s_3386/files/1379942540-sunpower_c60_bin_ghi.pdf (accessed on 18 July 2024).
43. Spectrolab, Inc. GaAs/Ge Single Junction Solar Cells. Available online: https://www.spectrolab.com/DataSheets/SJCell/sj.pdf (accessed on 18 July 2024).
44. Spectrolab, Inc. NeXt Triple Junction (XTJ) Solar Cells. Available online: https://www.spectrolab.com/DataSheets/cells/PV%20XTJ%20Cell%205-20-10.pdf (accessed on 18 July 2024).
45. TDK Corporation. Thin-Film Solar Cell. Available online: https://product.tdk.com/system/files/dam/doc/product/solar-cell/catalog/film-solarcell_bcs_en.pdf (accessed on 18 July 2024).
46. Mohamed, H.A.; Khattab, H.A.; Mobarka, A.; Morsy, G.A. Design, Control and Performance Analysis of DC-DC Boost Converter for Stand-Alone PV System. In Proceedings of the 2016 Eighteenth International Middle East Power Systems Conference (MEPCON), IEEE, Cairo, Egypt, 27–29 December 2016; pp. 101–106.
47. Jain, S.K. High Efficiency DC-DC Boost Converter Using Solar Energy (PV) System. 2018, 6. Available online: https://www.google.com.hk/url?sa=t&source=web&rct=j&opi=89978449&url=https://ijcrt.org/papers/IJCRT1813187.pdf&ved=2ahUKEwjK-OaV6dGLAxUmqFYBHboJKH4QFnoECBMQAQ&usg=AOvVaw3iDB2cbE1DrRpx8fBqo-IC (accessed on 1 February 2025).
48. Gray, J.S.; Hwang, J.T.; Martins, J.R.R.A.; Moore, K.T.; Naylor, B.A. OpenMDAO: An Open-Source Framework for Multidisciplinary Design, Analysis, and Optimization. *Struct. Multidiscip. Optim.* **2019**, *59*, 1075–1104. [CrossRef]
49. Delbecq, S.; Budinger, M.; Reysset, A. Benchmarking of Monolithic MDO Formulations and Derivative Computation Techniques Using OpenMDAO. *Struct. Multidiscip. Optim.* **2020**, *62*, 645–666. [CrossRef]
50. DHC-2 Beaver Pilot's Manual, Version 1.02. Available online: https://milviz.com/Online_products/Manuals/MilViz_DHC2_Pilot's_Manual_v1.02.pdf (accessed on 16 December 2024).
51. Heit, Z.; Liscouet-Hanke, S. Estimation of Battery Pack Layout and Dimensions for the Conceptual Design of Hybrid-Electric Aircraft. In Proceedings of the AIAA SciTech 2023 Forum, National Harbor, MD, USA, 19 January 2023.
52. Victron Energy B.V. SmartSolar Charge Controller/MPPT. Available online: https://www.victronenergy.com/upload/documents/Datasheet-SmartSolar-charge-controller-MPPT-150-60-&-150-70-EN.pdf (accessed on 18 July 2024).
53. Remington Industries. Solid Copper Wire & Magnet Wire Data by AWG. Available online: https://www.remingtonindustries.com/content/Remington%20Copper%20and%20Magnet%20Wire%20Data%20Chart.pdf?srsltid=AfmBOoqb4_iQcKIX61EXvrRGdD4ogkKVJn6hEw9mWj_o_4Ft4r0DiHdA (accessed on 18 July 2024).

Disclaimer/Publisher's Note: The statements, opinions and data contained in all publications are solely those of the individual author(s) and contributor(s) and not of MDPI and/or the editor(s). MDPI and/or the editor(s) disclaim responsibility for any injury to people or property resulting from any ideas, methods, instructions or products referred to in the content.